Molecular Transport Junctions with Semiconductor Electrodes: Analytical Forms for One-Dimensional Self-Energies†

Matthew G. Reuter, Thorsten Hansen, Tamar Seideman, and Mark A. Ratner*

Department of Chemistry, Northwestern University, Evanston, Illinois 60208-3113

Received: December 30, 2008; Revised Manuscript Received: January 29, 2009

Analytical self-energies for molecular interfaces with one-dimensional, tight-binding semiconductors are derived, along with analytical solutions to the electrode eigensystems. These models capture the fundamental differences between the transport properties of metals and semiconductors and also account for the appearance of surface states. When the models are applied to zero-temperature electrode−molecule−electrode conductance, junctions with two semiconductor electrodes exhibit a minimum bias threshold for generating current due to the absence of electrode states near the Fermi level. Molecular interactions with semiconductor electrodes additionally produce (i) non-negligible molecular-level shifting by mechanisms absent in metals and (ii) sensitivity of the transport to the semiconductor−molecule bonding configuration. Finally, the general effects of surface states on molecular transport are discussed.

Introduction

The transfer of charge between an adsorbed molecule and a bulk substrate is a key process in a wide range of chemical reactions. For example, charge separation in dye-sensitized solar cells occurs at the interface of dye molecules and titanium dioxide nanoparticles.[1] Electrochemical processes additionally occur at metal surfaces.[2] Substrate−molecule interactions, useful for both their fundamental importance and their potential applications, clearly need to be understood.

A typical scanning tunneling microscopy experiment brings a metal tip into the vicinity of a surface-adsorbed molecule, where, under bias, current flows through the molecule as it traverses the tip−substrate gap. The past decade has witnessed immense interest in such molecular transport situations,[3−7] and most work in molecular electronics has emphasized the critical importance of the molecule−electrode interfaces.[8−14] Not only does the electronic coupling between the molecule and the surface control the magnitude of the current, it also influences the electronic structure of the molecule.

To date, theoretical descriptions, and to a lesser extent experimental efforts, have largely focused on systems with two metal electrodes,[8−11,13−17] often gold. Interesting physics, however, appears when one or both leads are replaced with semiconductors,[18−25] including negative differential resistance[19,20] and rectification.[18] The industrial dominance of semiconductors, notably silicon, suggests the development of hybrid electronics, where single molecules or organic thin films are integrated with conventional silicon technology.[26−29] Semiconductor surfaces with adsorbed molecules often lend themselves to near-perfect characterization and, with clever choices of semiconductor materials and dopants, permit customization of the band structure and transport properties to the specific application. Semiconductors also introduce mechanisms for interesting molecular vibrational dynamics, along with approaches for optical control.[30]

A detailed understanding of molecule−electrode coupling requires more than the simple tunneling barrier view of the transport junction. In the coherent tunneling regime, the tunneling current is often well-described by the Landauer−Imry equation,[31−33] where the molecule is treated using Green's functions. The molecule−surface interactions are indirectly described by the impact they have on the molecule, which is formally accomplished by a self-energy,

$$\Sigma(E) = \Lambda(E) - \frac{i}{2}\Gamma(E) \tag{1}$$

that modifies the molecular Green's functions. The real part of the self-energy, $\Lambda(E)$, describes the shift of a molecular energy level due to hybridization with the electrode. This molecular level shifting is negligible for metals[11] in the wide band limit; however, recent studies have shown molecule−semiconductor interactions to be more significant.[22,25] The spectral density, $\Gamma(E)$, represents the broadening of a molecular level induced by the electrode and is effectively the density of electrode states weighted by the square of the molecule−electrode coupling. The self-energy also captures the effects of surface states.

Contemporary computational approaches use electronic structure calculations of the self-energies for investigating molecular transport junctions.[8,10,11,15,23,24,34,35] These approaches, while broadly applicable, can be complicated by the treatment of electron correlation and by basis set errors, and additionally by band bending and by doping when semiconductors are considered. At the expense of quantitative accuracy, much physical insight can be gained from analytical models of the self-energy. Newns[36] derived a simple analytical model for the self-energy of an interface between a molecule and a one-dimensional, tight-binding metal electrode, building on earlier work by Anderson.[37] The introduction of alternating site energies or intersite couplings has generalized this metal model to one-dimensional semiconductors, where such alternations yield band gaps in the models' densities of states.[38−40]

This is the starting point for our work. Following Newns, we derive an analytical expression for the self-energy of a

† Part of the "George C. Schatz Festschrift".

* To whom correspondence should be addressed. E-mail: ratner@northwestern.edu.

10.1021/jp811492u CCC: $40.75
Published on Web 03/26/2009

semiconductor−molecule interface where the lead has simultaneously alternating site energies and intersite couplings. We subsequently investigate the current−voltage characteristics of model molecular transport junctions with various metal and semiconductor electrodes. Previous work[41] treated two limits of this model where only the site energies or only the intersite couplings were alternated. As was noted, those results did not correctly coincide with the Newns−Anderson result in the limit of metal electrodes. This work solves the model in full generality, correcting these deficiencies, and exposes the consequences of some assumptions made in ref 41 by comparing the appropriate limits.

The layout of this paper is as follows. We first review the basics of molecular conductance, the Newns−Anderson (NA) model for metals, and the essentials of surface states. We then solve the various semiconductor electrodes' eigensystems, derive the semiconductor−molecule interfaces' self-energies, and compare the appropriate limits to the results of the previous article. We proceed to examine how semiconductor electrodes and their molecule−substrate interactions influence current−voltage curves, as opposed to those of metal electrodes. We finally draw several conclusions and suggest ideas for future studies.

Electronic Transport, Models, and Surface States

Molecular Conductance. When a molecule adsorbs to a surface or attaches to an electrode, the molecular energy levels both shift and broaden into resonances, as described by the self-energy. Here, we assume that the molecule has only a single state, $|s\rangle$, of energy ε, representing a broad class of molecular systems where only one or two molecular states contribute as channels toward the total conductance. This assumption is acceptable since molecular-level spacings are usually large and is convenient for investigating the essential physics underlying charge-transfer processes.

We denote the "atomic" levels of a particular electrode by $\{|\chi_j\rangle\}$ and the Bloch states of the same electrode by $\{|k\rangle\}$ with corresponding energies $\{\varepsilon_k\}$. In a tight-binding picture where each electrode site has only a single level, the molecular state solely couples to the terminal atomic level, $|\chi_1\rangle$, that is, $\langle s|\mathscr{H}|\chi_j\rangle = \gamma\delta_{j,1}$, where $\mathscr{H}$ is the total system Hamiltonian. For isolated resonances, the spectral density resulting from adsorption is

$$\Gamma(E) = 2\pi \sum_k |V_k|^2 \delta(E - \varepsilon_k) \tag{2}$$

with $V_k \equiv \langle s|\mathscr{H}|k\rangle = \gamma\langle\chi_1|k\rangle$. When $\Sigma(E)$ has no singularities on the real energy axis, $\Gamma(E)$ is related to $\Lambda(E)$ by the Hilbert transform, which is often nontrivial to evaluate analytically. As we will see, such singularities may be manifestations of electrode surface states.

Alternatively, the self-energy of a molecule coupled to an electrode can be expressed in terms of the electrode Green's function:

$$\Sigma(E) = V^\dagger G_{\text{elec}}(E) V \tag{3}$$

where V is the molecule−electrode coupling matrix and $G_{\text{elec}}(E)$ is the electrode Green's function. In a one-dimensional, tight-binding picture,[42,43]

$$G^i_{\text{elec}}(E) = \frac{1}{E - \alpha_i - \beta_i^2 G^{i+1}_{\text{elec}}(E)} \tag{4}$$

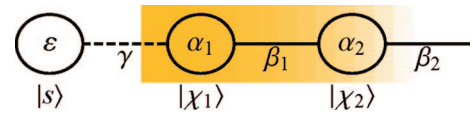

Figure 1. Schematic display of the general one-dimensional, tight-binding system. The site energy of $|\chi_i\rangle$ is α_i, and the coupling element between $|\chi_i\rangle$ and $|\chi_{i+1}\rangle$ is β_i. The molecular level $|s\rangle$ has energy ε and couples to $|\chi_1\rangle$ with element γ.

where the superscripts denote the specific site in the one-dimensional chain;[44] α_i is the site energy of site i, and β_i is the coupling element between sites i and $i + 1$. We assume all $\beta_i < 0$, restricting our attention to bonding-type overlaps, and that all α_i are real. Extensions incorporating antibonding-type overlaps ($\beta_i > 0$) are easily performed. Figure 1 schematically represents such a one-dimensional electrode. For the systems appearing later, this formulation provides the real and imaginary parts of $\Sigma(E)$ up to a choice of sign, vide infra. The subsequent calculations will also be simplified if we require the average site energy of all electrode sites, ξ, to be 0, thereby making the α_i into relative energies. We will replace E by $E - \xi$ for scenarios where ξ plays a more prominent role.

In the Landauer−Imry limit,[31−33] the transmission function for an electron injected into the electrode−molecule−electrode junction at energy E is

$$T(E) = \text{Tr}[\Gamma_L(E) G(E) \Gamma_R(E) G^\dagger(E)]$$

which simplifies to

$$T(E) = |G(E)|^2 \Gamma_L(E) \Gamma_R(E) \tag{5}$$

when the molecule has a single state. In eq 5, $\Gamma_{L(R)}(E)$ is the spectral density from coupling to the left (right) electrode, $G(E)$ is the retarded molecular Green's function,

$$G(E) = \frac{1}{E - \varepsilon - \Sigma_L(E) - \Sigma_R(E)} \tag{6}$$

ε is the molecular state energy, and $\Sigma_{L(R)}(E)$ is the self-energy from coupling to the left (right) electrode. For isolated resonances and noninteracting electrodes (except via the molecule), the transmission function at a molecular energy level, $T(\varepsilon)$, will have a Lorentzian line shape with width Γ. We note that $T(E)$ parametrically depends on an applied bias voltage V, $T = T(E; V)$, since the bias shifts the electrode levels, thereby altering the self-energies and molecular Green's function.

Suppose that the left electrode has a Fermi level $E_{F,L}$ and that the right electrode's is $E_{F,R}$. When the electrode−molecule−electrode junction is initially connected, electrons spontaneously flow (without an applied bias) from high free-energy states in one electrode to lower free-energy states in the other via the molecule. This charge transfer between the electrodes contributes an electrostatic potential difference across the junction, which increases until the effective Fermi levels of the two electrodes equalize and the system reaches equilibrium. This equilibrium Fermi level, E_F, is not trivial to calculate and is one facet of the "band lineup" problem.[45] The other aspect pertains to the amount of charge transferred between the electrodes. For simplicity, we circumvent this problem by requiring electrodes to be of the same material, $E_{F,L} = E_{F,R} = E_F$ and the system is in equilibrium at zero bias.

The total current through the junction, I, is[34,46]

$$I(V) = \frac{2e}{h}\int_{-\infty}^{\infty} \mathrm{d}E T(E;V)[f_{\mathrm{L}}(E;V) - f_{\mathrm{R}}(E;V)] \qquad (7)$$

where $f_{\mathrm{L(R)}}(E;V)$ is the Fermi function of the left (right) electrode. Each Fermi function depends on the electrode's chemical potential, which in turn relies on the applied bias. Two limits allow simplifications of eq 7. First is the limit of zero temperature, $f_{\mathrm{L(R)}}(E;V) \rightarrow \Theta(-E + E_{\mathrm{F}} \pm eV/2)$, where $\Theta(x)$ is the Heaviside (step) function. The use of plus/minus signs here arises from the arbitrary "left" and "right" labels applied to the electrodes. The second is the small bias limit, where we neglect the transmission function's dependence on the bias, $T(E;V) \rightarrow T(E)$. Applying these limits,

$$I(V) = \frac{2e}{h}\int_{E_{\mathrm{F}}-eV/2}^{E_{\mathrm{F}}+eV/2} \mathrm{d}E T(E) \qquad (8)$$

Newns−Anderson (NA) Metal Model. A concise review of the Newns−Anderson model will prove indispensable in the derivations presented later. Representing a chain of N identical metal sites in a tight-binding picture, the Newns−Anderson Hamiltonian is

$$\mathscr{H}_{\mathrm{NA}} = \beta \sum_{j=1}^{N-1} |\chi_j\rangle\langle\chi_{j+1}| + \mathrm{h.c.} \qquad (9)$$

All of the atomic levels here have the same energy, allowing us to take $\alpha_i = 0$ without any loss in generality ($\xi = 0$). From Bloch's theory, we expect the eigenstates of $\mathscr{H}_{\mathrm{NA}}$ to be

$$\begin{aligned} |k\rangle &= A|k^+\rangle + B|k^-\rangle \\ &= A\sum_{j=1}^{N} \mathrm{e}^{ikj}|\chi_j\rangle + B\sum_{j=1}^{N} \mathrm{e}^{-ikj}|\chi_j\rangle \end{aligned} \qquad (10)$$

for constants A and B. Clearly, $\langle\chi_j|k\rangle = A\mathrm{e}^{ikj} + B\mathrm{e}^{-ikj}$.

To determine A and B, we create virtual sites 0 and $N + 1$ such that the eigenstate amplitude disappears at these sites, $\langle\chi_0|k\rangle = \langle\chi_{N+1}|k\rangle = 0$. From these conditions, we see that k is quantized, $k = k_n = n\pi/(N + 1)$, with $n = 1, 2, ..., N$, that

$$|k_n\rangle = \sqrt{\frac{2}{N+1}}\sum_{j=1}^{N} \sin(k_n j)|\chi_j\rangle \qquad (11)$$

once normalized, and that $\varepsilon_{k_n} = 2\beta\cos(k_n)$ is the eigenvalue of $|k_n\rangle$.

The eigenstates, with $V_{k_n} = 2^{1/2}(N + 1)^{-1/2}\gamma\sin(k_n)$, and eq 2 are used to determine $\Gamma_{\mathrm{NA}}(E)$. In the limit of $N \rightarrow \infty$, where k_n essentially becomes continuous,

$$\begin{aligned} \Gamma_{\mathrm{NA}}(E) &= \lim_{N\rightarrow\infty} 2\pi\sum_{n=1}^{N}\frac{2\gamma^2}{N+1}\sin^2(k_n)\delta(E - 2\beta\cos(k_n)) \\ &= 4\gamma^2\int_0^{\pi}\mathrm{d}k\sin^2(k)\delta(E - 2\beta\cos(k)) \\ &= \frac{\gamma^2}{\beta^2}\sqrt{4\beta^2 - E^2} \end{aligned} \qquad (12)$$

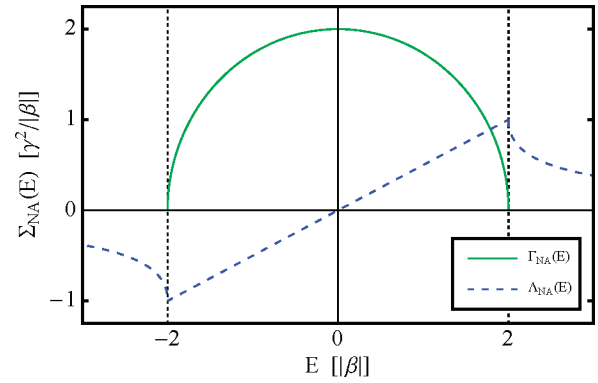

Figure 2. The self-energy, $\Sigma_{\mathrm{NA}}(E)$, for a molecule and a Newns−Anderson metal. $\Gamma_{\mathrm{NA}}(E)$ (green, solid line) peaks at $E = 0$ to a value of $2\gamma^2/|\beta|$, and $\Lambda_{\mathrm{NA}}(E)$ (blue, dashed line) realizes its extrema of $\pm\gamma^2/|\beta|$ at $E = \pm 2|\beta|$.

for $|E| \leq 2|\beta|$. $\Gamma_{\mathrm{NA}}(E) = 0$ for all other E. The center of the metal band is ξ, and the bandwidth is $4|\beta|$.

We now use the electrode Green's function formulation of $\Sigma_{\mathrm{NA}}(E)$ to determine $\Lambda_{\mathrm{NA}}(E)$. Since all sites in this one-dimensional chain are identical, eq 4 becomes

$$G^i_{\mathrm{NA}}(E) = \frac{1}{E - \beta^2 G^i_{\mathrm{NA}}(E)}$$

which produces (dropping the superscript)

$$G_{\mathrm{NA}}(E) = \frac{E \pm \sqrt{E^2 - 4\beta^2}}{2\beta^2} \qquad (13)$$

As foreshadowed earlier, we obtain $G_{\mathrm{NA}}(E)$ up to a choice of sign. $G_{\mathrm{NA}}(E)$ is complex when $E^2 - 4\beta^2 < 0$ ($|E| < 2|\beta|$), and the negative sign is chosen to make $\Gamma_{\mathrm{NA}}(E) \geq 0$; see eqs 1 and 2. Parenthetically, this choice yields eq 12 once we introduce the two factors of γ from V and $V^{\dagger}$.

When the molecular site level is energetically far from the metal band, we expect the surface to induce negligible molecular effects, that is, $\Sigma_{\mathrm{NA}}(E) \rightarrow 0$ as $|E| \rightarrow \infty$. Only one sign choice for each interval, $E < -2|\beta|$ and $E > 2|\beta|$, satisfies this requirement, allowing the total specification

$$\frac{\Lambda_{\mathrm{NA}}(E)}{\gamma^2} = \frac{E}{2\beta^2} + \Theta_{\mathrm{NA}}(E)\frac{\sqrt{E^2 - 4\beta^2}}{2\beta^2} \qquad (14)$$

where

$$\Theta_{\mathrm{NA}}(E) = \Theta(-2|\beta| - E) - \Theta(E - 2|\beta|)$$

We note that $\Theta_{\mathrm{NA}}(E)$ specifies the sign choices and that, for this simple model, the Hilbert transform of $\Gamma_{\mathrm{NA}}(E)$ can be analytically evaluated, yielding the same result. Figure 2 shows $\Lambda_{\mathrm{NA}}(E)$ and $\Gamma_{\mathrm{NA}}(E)$.

Semiconductor Models. Several perturbations of the Newns−Anderson metal model have been used for modeling semiconductors.[38−41,47,48] One such model, introduced by Koutecký and Davison (KD),[38] alternates both the site energies and intersite couplings, doubling the unit cell of the one-dimensional crystal. This model may consider each unit cell as an atom,

with the two sites' states corresponding to s and p orbitals. The coupling between the s and p orbitals in the same unit cell describes their overlap, and the coupling across unit cells describes the interatomic bonding. Neighboring s−s and p−p interactions are neglected in the simple tight-binding model. For convenience, we will assume there are $2N$ atomic sites in the system, a moot distinction in the limit of $N \rightarrow \infty$. The Hamiltonian for this system is

$$\mathscr{H}_{\mathrm{KD}} = \alpha \sum_{j=1}^{N} |\chi_{2j-1}\rangle\langle\chi_{2j-1}| - \alpha \sum_{j=1}^{N} |\chi_{2j}\rangle\langle\chi_{2j}| + [\beta_1 \sum_{j=1}^{N} |\chi_{2j-1}\rangle\langle\chi_{2j}| + \beta_2 \sum_{j=1}^{N-1} |\chi_{2j+1}\rangle\langle\chi_{2j}| + \mathrm{h.c.}] \quad (15)$$

The restriction $\xi = 0$ here allows a reduction in the number of parameters; only one (α) is needed to describe the disparate site energies (α and $-\alpha$), as opposed to the more general case requiring two.

The KD model has three important limits. First is the combined limit $\alpha \rightarrow 0$ and $\beta_1 \rightarrow \beta_2 \equiv \beta$, which produces the Newns−Anderson model. Second is the limit $\beta_1 \rightarrow \beta_2 \equiv \beta$. This alternating site (AS) model has been used to describe titanium dioxide,[40] where the site energies (α and $-\alpha$) correspond to the different atoms. The AS Hamiltonian ($\xi = 0$) is

$$\mathscr{H}_{\mathrm{AS}} = \alpha \sum_{j=1}^{N} |\chi_{2j-1}\rangle\langle\chi_{2j-1}| - \alpha \sum_{j=1}^{N} |\chi_{2j}\rangle\langle\chi_{2j}| + [\beta \sum_{j=1}^{2N-1} |\chi_j\rangle\langle\chi_{j+1}| + \mathrm{h.c.}] \quad (16)$$

Lastly is the limit $\alpha \rightarrow 0$, where the model alternates bonds (AB). The AB model has been used to model silicon and germanium,[39] where the bond disparities (β_1 and β_2) relate to orbital hybridization (the s and p orbitals become degenerate, as is the case when they hybridize). The AB Hamiltonian ($\xi = 0$) is

$$\mathscr{H}_{\mathrm{AB}} = \beta_1 \sum_{j=1}^{N} |\chi_{2j-1}\rangle\langle\chi_{2j}| + \beta_2 \sum_{j=1}^{N-1} |\chi_{2j+1}\rangle\langle\chi_{2j}| + \mathrm{h.c.} \quad (17)$$

Surface States. When a crystal is cleaved into two noninteracting parts, symmetries break and surfaces form. The surfaces can exhibit dangling bonds, potentially leading to reconstructions, and surface states, with densities localized near the surface. Two principal types of surface states, Tamm[49] and Shockley[50] states, are very similar in effect but caused by different physics. Tamm states appear when the site energies and intersite couplings near the surface are sufficiently perturbed from their bulk values. These perturbations are collectively called the surface potential. Alternatively, Shockley states result from band "crossings" and appear in the gap between crossed bands. Additional contrasts between Tamm and Shockley surface states are discussed in refs 38 and 47. With no surface potential in the KD model (also AB and AS), any surface states here will be of the Shockley type.

Surface states are properties of the electrode alone, as opposed to the molecule−electrode interface, and can be identified by any poles of the electrode Green's function.[51] Koutecký calculated that a surface state appears in the KD model at $E = \alpha$ when $|\beta_1| \leq |\beta_2|$.[38] It follows that a surface state also appears at $E = 0$ when $|\beta_1| < |\beta_2|$ in the AB model. In these cases, the localized bond between sites 0 and 1 is of the stronger bond type and creates a surface state of nonbonding character when it ruptures during surface formation.[38] Furthermore, this surface state moves to a band edge at $E = \alpha$ in the AS model ($\beta_1 = \beta_2$), representing the point of band crossing. A surface state does not appear when a weaker bond is broken ($|\beta_1| > |\beta_2|$). As a small digression, the surface states for these one-dimensional models can also be termed end states. Just as two-dimensional surface states appear for three-dimensional solids, these end states are zero-dimensional, only having densities at the ends of the chain. Experiments have recently observed such end states.[52]

Semiconductor−Molecule Self-Energies

The derivation of the self-energy for the Koutecký−Davison (KD) semiconductor−molecule interface will follow the methodology of the Newns−Anderson (NA) metal−molecule interface: we solve the Hamiltonian eigensystem and use its solutions to calculate the spectral density. We then obtain $\Lambda_{\mathrm{KD}}(E)$ by the electrode Green's function method. We finally take the limits $\alpha \rightarrow 0$ and $\beta_1 \rightarrow \beta_2 \equiv \beta$ to explore AB and AS junctions, respectively.

Koutecký−Davison (KD) Model. The two-fold alternation of the sites suggests that two Bloch states are required for describing the system. If we first restrict our attention to outgoing states (scattering states obeying retarded boundary conditions, denoted by a + superscript), these two states are

$$|k^{+,\mathrm{o}}\rangle = \frac{1}{\sqrt{N}} \sum_{j=1}^{N} \mathrm{e}^{ik(2j-1)} |\chi_{2j-1}\rangle$$

and

$$|k^{+,\mathrm{e}}\rangle = \frac{1}{\sqrt{N}} \sum_{j=1}^{N} \mathrm{e}^{ik2j} |\chi_{2j}\rangle$$

where $|k^+\rangle = C_{\mathrm{o}}|k^{+,\mathrm{o}}\rangle + C_{\mathrm{e}}|k^{+,\mathrm{e}}\rangle$. Since we want $|k^+\rangle$ to be an eigenstate of $\mathscr{H}_{\mathrm{KD}}$, we solve the secular equation,

$$0 = \begin{vmatrix} \langle k^{+,\mathrm{o}}|\mathscr{H}_{\mathrm{KD}}|k^{+,\mathrm{o}}\rangle - \varepsilon & \langle k^{+,\mathrm{o}}|\mathscr{H}_{\mathrm{KD}}|k^{+,\mathrm{e}}\rangle \\ \langle k^{+,\mathrm{e}}|\mathscr{H}_{\mathrm{KD}}|k^{+,\mathrm{o}}\rangle & \langle k^{+,\mathrm{e}}|\mathscr{H}_{\mathrm{KD}}|k^{+,\mathrm{e}}\rangle - \varepsilon \end{vmatrix} = \begin{vmatrix} \alpha - \varepsilon & \beta_1 \mathrm{e}^{ik} + \beta_2 \mathrm{e}^{-ik} \\ \beta_1 \mathrm{e}^{-ik} + \beta_2 \mathrm{e}^{ik} & -\alpha - \varepsilon \end{vmatrix}$$

to find that

$$\varepsilon_k^2 = \alpha^2 + \beta_1^2 + \beta_2^2 + 2\beta_1\beta_2 \cos(2k)$$
$$\varepsilon_k = \mathrm{sign}[\cos(k)]\sqrt{\alpha^2 + \beta_1^2 + \beta_2^2 + 2\beta_1\beta_2 \cos(2k)} \quad (18)$$

The sign function in eq 18 forces both the density of states (not shown) and the spectral density (vide infra) to remain nonnegative for all E, as required by definition and eq 2, respectively. Using these eigenvalues, the secular equation, and the normalization condition $|C_{\mathrm{o}}|^2 + |C_{\mathrm{e}}|^2 = 1$, we determine the outgoing eigenstates as

$$|k^+\rangle = \frac{(\beta_1 e^{ik} + \beta_2 e^{-ik})|k^{+,o}\rangle + (\varepsilon_k - \alpha)|k^{+,e}\rangle}{\sqrt{(\varepsilon_k - \alpha)^2 + \beta_1^2 + \beta_2^2 + 2\beta_1\beta_2 \cos(2k)}} = \frac{1}{\sqrt{N}}\sum_{j=1}^{N} \frac{(\beta_1 e^{ik} + \beta_2 e^{-ik})e^{ik(2j-1)}|\chi_{2j-1}\rangle + (\varepsilon_k - \alpha)e^{ik2j}|\chi_{2j}\rangle}{\sqrt{(\varepsilon_k - \alpha)^2 + \beta_1^2 + \beta_2^2 + 2\beta_1\beta_2 \cos(2k)}} \quad (19)$$

We obtain the incoming eigenstate equivalent,

$$|k^-\rangle = \frac{1}{\sqrt{N}}\sum_{j=1}^{N} \frac{(\beta_1 e^{-ik} + \beta_2 e^{ik})e^{-ik(2j-1)}|\chi_{2j-1}\rangle + (\varepsilon_k - \alpha)e^{-ik2j}|\chi_{2j}\rangle}{\sqrt{(\varepsilon_k - \alpha)^2 + \beta_1^2 + \beta_2^2 + 2\beta_1\beta_2 \cos(2k)}}$$

from a very similar process.

Following the Newns−Anderson approach, we write the Hamiltonian eigenstates as $|k\rangle = A|k^+\rangle + B|k^-\rangle$, where

$$\langle\chi_{2j-1}|k\rangle = \frac{A(\beta_1 e^{ik} + \beta_2 e^{-ik})e^{ik(2j-1)} + B(\beta_1 e^{-ik} + \beta_2 e^{ik})e^{-ik(2j-1)}}{\sqrt{N}\sqrt{(\varepsilon_k - \alpha)^2 + \beta_1^2 + \beta_2^2 + 2\beta_1\beta_2 \cos(2k)}}$$

$$\langle\chi_{2j}|k\rangle = \frac{(\varepsilon_k - \alpha)(Ae^{ik2j} + Be^{-ik2j})}{\sqrt{N}\sqrt{(\varepsilon_k - \alpha)^2 + \beta_1^2 + \beta_2^2 + 2\beta_1\beta_2 \cos(2k)}}$$

Again introducing the virtual sites 0 and $2N + 1$ such that $(\chi_0|k\rangle = (\chi_{2N+1}|k\rangle = 0$, we see that

$$\langle\chi_{2j-1}|k_n\rangle = \frac{2A}{\sqrt{N}}\frac{\beta_1 \sin[2k_n j] + \beta_2 \sin[2k_n(j-1)]}{\sqrt{(\varepsilon_{k_n} - \alpha)^2 + \beta_1^2 + \beta_2^2 + 2\beta_1\beta_2 \cos(2k_n)}}$$

$$\langle\chi_{2j}|k_n\rangle = \frac{2A}{\sqrt{N}}\frac{(\varepsilon_{k_n} - \alpha)\sin(2k_n j)}{\sqrt{(\varepsilon_{k_n} - \alpha)^2 + \beta_1^2 + \beta_2^2 + 2\beta_1\beta_2 \cos(2k_n)}}$$

where k is quantized by

$$\beta_1 \sin[2k_n(N+1)] + \beta_2 \sin[2k_n N] = 0 \quad (20)$$

with $n = 1, 2, ..., 2N$. An additional solution with $\varepsilon = \alpha$ can arise from $\langle\chi_0|k\rangle = 0$, indicating the possible presence of the surface state.

The Hamiltonian eigenstates are then

$$|k_n\rangle = A_{k_n}\sum_{j=1}^{N} \frac{(\beta_1 \sin[2k_n j] + \beta_2 \sin[2k_n(j-1)])|\chi_{2j-1}\rangle + (\varepsilon_{k_n} - \alpha)\sin(2k_n j)|\chi_{2j}\rangle}{\sqrt{(\varepsilon_{k_n} - \alpha)^2 + \beta_1^2 + \beta_2^2 + 2\beta_1\beta_2 \cos(2k_n)}} \quad (21)$$

where A_{k_n} is the normalization constant. For the case where $\beta_1 = \beta_2$, the k_n satisfy $k_n = n\pi/(2N + 1)$ and $A_{k_n} = 2/(2N + 1)^{1/2}$ (an equivalent quantization condition to the Newns−Anderson case for $2N$ sites, after simplification).[53] Even though changes in β_1 and β_2 vary the spacings between the k_n, we will assume they are uniform (and hence the normalization constants are invariant) for the spectral density calculation.[54] This assumption is needed for the conversion of a discrete sum to a continuous integral.

Having the eigenvalues and the eigenvectors, the spectral density can be calculated using eq 2, as detailed in the Appendix. Accordingly

$$\Gamma_{KD}(E) = \frac{\gamma^2}{\beta_2^2}\sqrt{\frac{[\alpha^2 + (\beta_1 + \beta_2)^2 - E^2][E^2 - \alpha^2 - (\beta_1 - \beta_2)^2]}{(E - \alpha)^2}} \quad (22)$$

for $[\alpha^2 + (\beta_1 - \beta_2)^2]^{1/2} \leq |E| \leq [\alpha^2 + (\beta_1 + \beta_2)^2]^{1/2}$. $\Gamma_{KD}(E) = 0$ for all other E.

Here, we see that the center of the band gap is at $E = 0$, suggesting ξ represents the center of the band gap. We also note that $\Gamma_{KD}(E)$ simplifies to $\Gamma_{NA}(E)$ in the combined limit of $\alpha \to 0$ and $\beta_1 \to \beta_2 \equiv \beta$, as desired. For parametrization purposes, the band gap is given by $2[\alpha^2 + (\beta_1 - \beta_2)^2]^{1/2}$, and the valence (or conduction) band width is given by $[\alpha^2 + (\beta_1 + \beta_2)^2]^{1/2} - [\alpha^2 + (\beta_1 - \beta_2)^2]^{1/2}$. Having three parameters and two nonlinear conditions, there may be flexibility in choosing values, and a third criterion from the band structure may be prudent. One immediate limitation of this model is that the valence and conduction bands have equal band widths.

$\Gamma_{KD}(E)$ is also *asymmetric* with respect to the interchange of β_1 for β_2 and of α for $-\alpha$. For this β disparity, a careful review of the Hamiltonian shows that, for $2N$ sites, there is one more β_1 bond than there is β_2, demonstrating the difference between the two bond types. The sensitivity to α stresses the importance of the surface. As we will thoroughly explore later, these asymmetries hint at the importance of the molecule−semiconductor bonding configuration to the molecule−electrode interactions.

We now use eq 4 to deduce an analytic form for $\Lambda_{KD}(E)$. Due to the alternations, there are two electrode Green's functions: one for the odd-indexed sites and another for those even,

$$G^1_{KD}(E) = \frac{1}{E - \alpha - \beta_1^2 G^2_{KD}(E)}$$
$$G^2_{KD}(E) = \frac{1}{E + \alpha - \beta_2^2 G^1_{KD}(E)}$$

We only need $G^1_{KD}(E)$ for calculating $\Sigma_{KD}(E)$ since the molecule solely couples to site 1 in the tight-binding Hamiltonian (V is 0 for the other sites). Correspondingly

$$G^1_{KD}(E) = \frac{E^2 - \alpha^2 - \beta_1^2 + \beta_2^2 \pm \sqrt{[E^2 - \alpha^2 - (\beta_1 - \beta_2)^2][E^2 - \alpha^2 - (\beta_1 + \beta_2)^2]}}{2\beta_2^2(E - \alpha)} \tag{23}$$

Following the discussion for the NA model, we choose the positive radical for $-[\alpha^2 + (\beta_1 + \beta_2)^2]^{1/2} \le E \le -[\alpha^2 + (\beta_1 - \beta_2)^2]^{1/2}$ and the negative for $[\alpha^2 + (\beta_1 - \beta_2)^2]^{1/2} \le E \le [\alpha^2 + (\beta_1 + \beta_2)^2]^{1/2}$ to make $\Gamma_{KD}(E) \ge 0$. Similarly, the negative branch ensures that $\Sigma_{KD}(E) \to 0$ as $|E| \to \infty$.

The only remaining sign selection pertains to the band gap region. From Koutecký,[38] we expect a surface state at $E = \alpha$ only when $|\beta_1| \le |\beta_2|$. Translating to requirements of the Green's function, $G^1_{KD}(E)$ should have a pole at $E = \alpha$ when $|\beta_1| \le |\beta_2|$ and be well-behaved when $|\beta_1| > |\beta_2|$. The denominator of $G^1_{KD}(E)$ is irrefutably 0 at $E = \alpha$, meaning $G^1_{KD}(E)$ has a removable singularity when its numerator is 0 and a first-order pole otherwise. Furthermore, the radical simplifies to $|\beta_1^2 - \beta_2^2|$ at $E = \alpha$, making the positive branch the desired choice here for all combinations of β_1 and β_2. Finally

$$\frac{\Lambda_{KD}(E)}{\gamma^2} = \frac{E^2 - \alpha^2 - \beta_1^2 + \beta_2^2 + \Theta_{KD}(E)\sqrt{[E^2 - \alpha^2 - (\beta_1 - \beta_2)^2][E^2 - \alpha^2 - (\beta_1 + \beta_2)^2]}}{2\beta_2^2(E - \alpha)} \tag{24}$$

where

$$\Theta_{KD}(E) = \Theta(\alpha^2 + (\beta_1 - \beta_2)^2 - E^2) - \Theta(E^2 - \alpha^2 - (\beta_1 + \beta_2)^2)$$

As with $\Gamma_{KD}(E)$, $\Lambda_{KD}(E) \to \Lambda_{NA}(E)$ in the combined limit of $\alpha \to 0$ and $\beta_1 \to \beta_2 \equiv \beta$.[55]

Alternating Site (AS) and Alternating Bond (AB) Models. The above procedure could be repeated in the analysis of the AS and AB models; however, it is far easier to take the limits $\beta_1 \to \beta_2 \equiv \beta$ and $\alpha \to 0$, respectively. For the AS model, we get

$$\frac{\Gamma_{AS}(E)}{\gamma^2} = \frac{1}{\beta^2}\sqrt{\frac{(\alpha^2 + 4\beta^2 - E^2)(E + \alpha)}{E - \alpha}} \tag{25}$$

for $|\alpha| < |E| \le (\alpha^2 + 4\beta^2)^{1/2}$, and $\Gamma_{AS}(E) = 0$ otherwise. Similarly

$$\frac{\Lambda_{AS}(E)}{\gamma^2} = \frac{E^2 - \alpha^2 + \Theta_{AS}(E)\sqrt{(E^2 - \alpha^2)(E^2 - \alpha^2 - 4\beta^2)}}{2\beta^2(E - \alpha)} \tag{26}$$

with

$$\Theta_{AS}(E) = \Theta(\alpha^2 - E^2) - \Theta(E^2 - \alpha^2 - 4\beta^2)$$

Given the reduction in the number of parameters, a semiconductor material can be represented by choosing $2|\alpha|$ to be the band gap and $(\alpha^2 + 4\beta^2)^{1/2} - |\alpha|$ to be the valence (conductance) band width. We note that α is only specified in magnitude. As expected from Koutecký,[38] the bulk band edges have extended to $\pm\alpha$, and the pole in $\Sigma_{AS}(E)$ at $E = \alpha$ indicates the surface state. Figure 3 displays $\Sigma_{AS}(E)$ for positive and negative α, highlighting the dependence of the surface state's location on the site energy of the "surface".

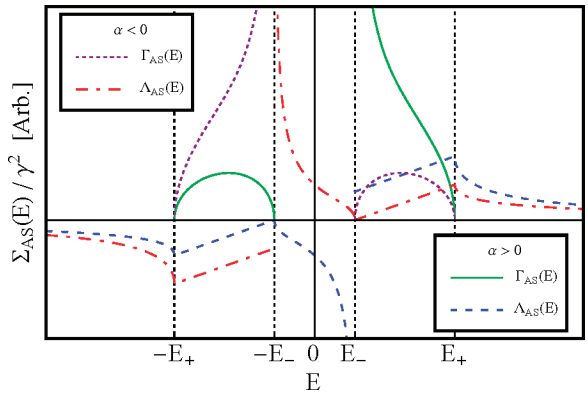

Figure 3. The self-energy, $\Sigma_{AS}(E)/\gamma^2$, for an interface with an AS semiconductor. The surface state at $E = \alpha$ manifests as a pole in both $\Gamma_{AS}(E)$ (green, solid line for $\alpha > 0$ or purple, dotted line for $\alpha < 0$) and $\Lambda_{AS}(E)$ (blue, dashed line for $\alpha > 0$ or red, dot−dashed line for $\alpha < 0$). The band edges are denoted, in magnitude, by $E_- \equiv |\alpha|$ and $E_+ \equiv (\alpha^2 + 4\beta^2)^{1/2}$.

Turning to the AB model,

$$\frac{\Gamma_{AB}(E)}{\gamma^2} = \frac{1}{\beta_2^2}\sqrt{\frac{[(\beta_1 + \beta_2)^2 - E^2][E^2 - (\beta_1 - \beta_2)^2]}{E^2}} \tag{27}$$

for $|\beta_1 - \beta_2| \le |E| \le |\beta_1 + \beta_2|$ and $\Gamma_{AB}(E) = 0$ otherwise. Additionally

$$\frac{\Lambda_{AB}(E)}{\gamma^2} = \frac{E^2 - \beta_1^2 + \beta_2^2 + \Theta_{AB}(E)\sqrt{(E^2 - (\beta_1 + \beta_2)^2)(E^2 - (\beta_1 - \beta_2)^2)}}{2\beta_2^2 E} \tag{28}$$

where

$$\Theta_{AB}(E) = \Theta((\beta_1 - \beta_2)^2 - E^2) - \Theta(E^2 - (\beta_1 + \beta_2)^2)$$

We can choose β_1 and β_2 such that $2|\beta_1 - \beta_2|$ is the material band gap and $|\beta_1 + \beta_2| - |\beta_1 - \beta_2|$ is the valence (conduction) band width. Similar to the AS model, these specifications ambiguously determine two β values for the material, β and β', with two ways to assign them to β_1 and β_2. Furthermore, the surface state expectedly appears at $E = 0$ when $|\beta_2| > |\beta_1|$. The existence of the surface state is the primary difference when β_1 and β_2 are interchanged, although the self-energy also scales with β_2^{-2}. Finally, Figure 4 depicts $\Sigma_{AB}(E)$ for both $|\beta_1| > |\beta_2|$ and $|\beta_1| < |\beta_2|$.

Comparison to Previous Results. A previous article[41] reported significantly different spectral densities for the AS and AB models from those reported here. In that derivation, the correct Bloch state energies were obtained; however, it was then assumed that $V_{k_n} \propto \sin(k_n)$ for the spectral density calculations, as was the case in the NA model. This assumption results in bands with the correct widths and gaps but incorrect structures. For comparison, these forms were

$$\frac{\Gamma_{AS}^{old}(E)}{\gamma^2} = \frac{2|E|}{\beta^2}\sqrt{1 - \left[\frac{E^2 - \alpha^2 - 2\beta^2}{2\beta^2}\right]^2} \tag{29}$$

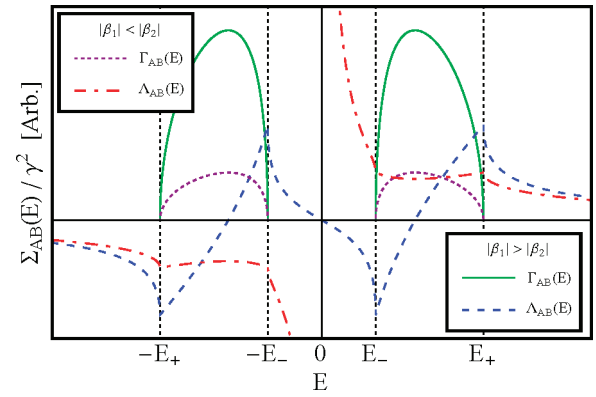

Figure 4. The self-energy, $\Sigma_{AB}(E)/\gamma^2$, for an interface with an AB semiconductor. When $|\beta_1| < |\beta_2|$, the surface state presents a pole in $\Lambda_{AB}(E)$ (red, dot−dashed line) at $E = 0$. $\Lambda_{AB}(E)$ is well-behaved at $E = 0$ when $|\beta_1| > |\beta_2|$ (blue, dashed line). The interchange of β_1 and β_2 simply rescales the spectral densities (the green, solid line for $|\beta_1| > |\beta_2|$ and the purple, dotted line for $|\beta_1| < |\beta_2|$). $E_- \equiv |\beta_1 - \beta_2|$ and $E_+ \equiv |\beta_1 + \beta_2|$ denote the band edges, in magnitude.

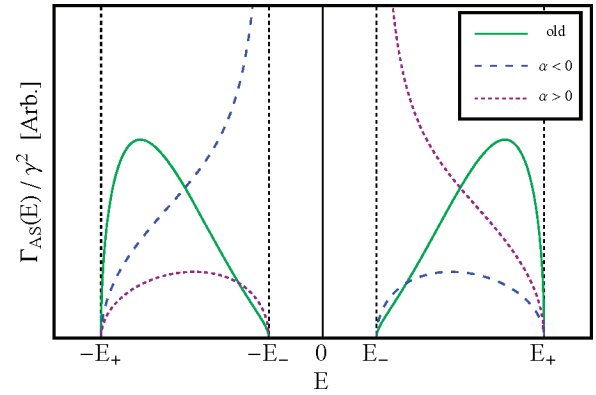

Figure 5. Comparison of $\Gamma_{AS}^{old}(E)/\gamma^2$ (green, solid line) with $\Gamma_{AS}(E)/\gamma^2$ for $\alpha < 0$ (blue, dashed line) and $\alpha > 0$ (purple, dotted line). As in Figure 3, $E_- \equiv |\alpha|$ and $E_+ \equiv (\alpha^2 + 4\beta^2)^{1/2}$.

and

$$\frac{\Gamma_{AB}^{old}(E)}{\gamma^2} = \frac{2|E|}{\beta_1\beta_2}\sqrt{1 - \left[\frac{E^2 - \beta_1^2 - \beta_2^2}{2\beta_1\beta_2}\right]^2} \tag{30}$$

We correct typographical errors in ref 41 by replacing E with $|E|$ in the numerators. Figures 5 and 6 display the old forms along with the new results presented here. In most cases, the old versions tend to overestimate the spectral densities, which could lead to inflated conductances, and they completely miss the surface states. The old versions are also symmetric with respect to the interchange of α for $-\alpha$ and β_1 for β_2.

Electronic Transport

Having computed the self-energies associated with these various models, we proceed to investigate the effects of semiconductor electrodes on electronic transport. The AB and AS models have been parametrized for various materials in the past, and values of α, β, and β' for gold, silicon, and titanium dioxide are listed in Table 1. We take ξ to be the material's Fermi level by assuming the metal band is half-filled[56] (we noted that ξ is the center of the band gap, the conventional Fermi level for semiconductors). Since all junctions have electrodes of the same material, we rescale the energy coordinate to $E_F =$

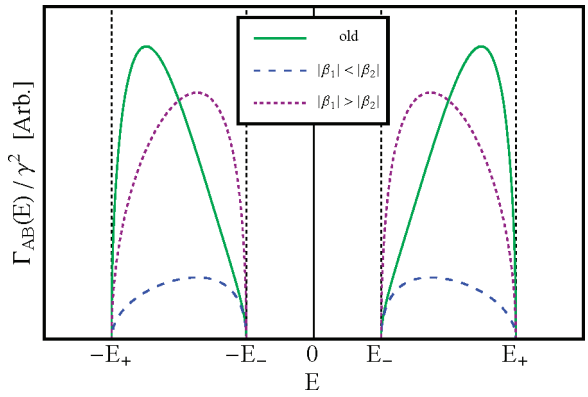

Figure 6. Comparison of $\Gamma_{AB}^{old}(E)/\gamma^2$ (green, solid line) with $\Gamma_{AB}(E)/\gamma^2$ for $|\beta_1| < |\beta_2|$ (blue, dashed line) and $|\beta_1| > |\beta_2|$ (purple, dotted line). As in Figure 4, $E_- \equiv |\beta_1 - \beta_2|$ and $E_+ \equiv |\beta_1 + \beta_2|$.

TABLE 1: Model Parameters for Au, Si, and TiO_2

material	model	$\|\alpha\|$ (eV)	β (eV)	β' (eV)	γ (eV)
Au[11]	NA		−8.95		−0.45
Si[39]	AB		−1.60	−2.185	−1.0
TiO_2[40]	AS	1.6	−2		−1.0

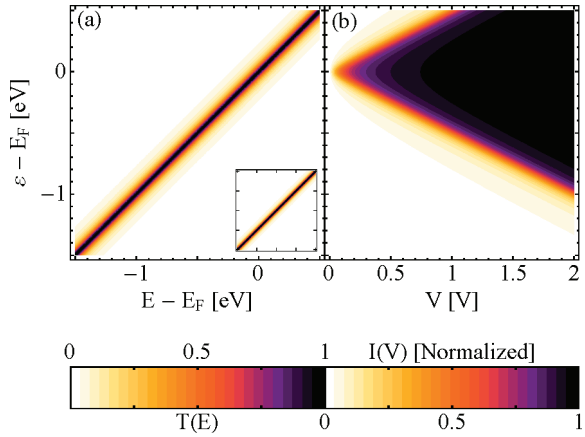

Figure 7. (a) Transmission and (b) current for two gold electrodes; see Table 1 for the parameterizations. The transmission with $\Lambda_{NA}(E)$ neglected [inset of (a)] is displayed for comparison, showing the molecular-level shifting described by $\Lambda_{NA}(E)$ to be insignificant for metals. The current is normalized to the maximum current in (b), which appears at $\varepsilon = E_F$.

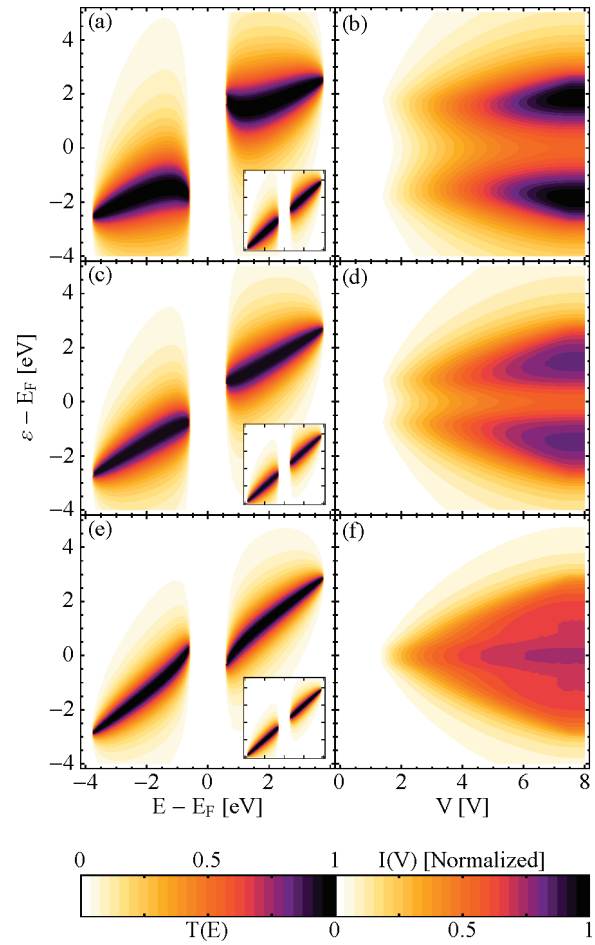

Figure 8. Transmissions (left column) and currents (right column) for junctions with two silicon electrodes. (a, b) $|\beta_2| < |\beta_1|$ for both electrodes (zero contributed surface states); (c, d) mixed β_1 and β_2 values for the two electrodes (one surface state); (e, f) $|\beta_2| > |\beta_1|$ for both electrodes (two surface states). The band gaps cause the strips of zero transmission around the Fermi level and the minimum bias thresholds for the existence of current. The insets of the transmission plots show the respective transmission functions when the molecular level shifting, $\Lambda_{AB}(E)$, is neglected. Unlike metals, such shiftings are important for semiconductors. The currents are normalized to the maximum current [which occurs in (b)], and the numerical parameter values are listed in Table 1.

0 ($\xi = 0$), highlighting the effects of α, β, and β'. We follow the convention of choosing $\gamma \approx \beta/2$ for TiO_2,[40] and similarly for Si. We pick γ for gold such that the magnitude of the metal spectral density is comparable to that in previous studies. Before applying the models, we warn against the quantitative interpretation of the ensuing results due to the qualitative selection of these critical parameters. To this end, the currents reported later will be normalized to the maximum current for a given set of electrodes in the particular calculation.

One paramount issue is the effect of semiconducting electrodes on the transport: how do semiconductors change the current−voltage profiles of electrode−molecule−electrode junctions? As a necessary basis for comparison, we briefly review the transport across a gold−molecule−gold junction, within the NA model and the Landauer−Imry limit. Figure 7 displays the transmission and current through the junction for various molecular-level energies, electron injection energies, and applied bias voltages. Figure 7a shows the formation of a resonance at each ε, as indicated by the ridge of high transmission. The resonances are present near the molecular state energies, although careful inspection reveals the high-transmission ridge (HTR) to be slightly perturbed from the $E = \varepsilon$ diagonal. The inset of Figure 7a shows the transmission function when we neglect the molecular-level shiftings caused by adsorption, $\Lambda_{NA}(E)$. With essentially unchanged results (the HTR remains linear, although now coincident with the $E = \varepsilon$ diagonal), we see that the weak molecular-level shiftings caused by adsorption to metals can be omitted to a good approximation (in agreement with ref 11). In Figure 7b, current appears for all positive voltages when the molecular site level is positioned at the Fermi energy, with increased voltages widening the range of molecular site levels able to function as current channels.

Two Semiconductor Electrodes. Having examined a metal−molecule−metal junction for comparison, we now consider semiconductor−molecule−semiconductor junctions within the AS and AB models. We first examine two silicon electrodes in the alternating bond framework. The semiconductor band gap is the most noticeable feature in the transmission plots (left column) of Figure 8, as evidenced by the vertical strip of zero transmission in each plot. In these regions, the absence of states in the donor electrode prevents electrons from injecting

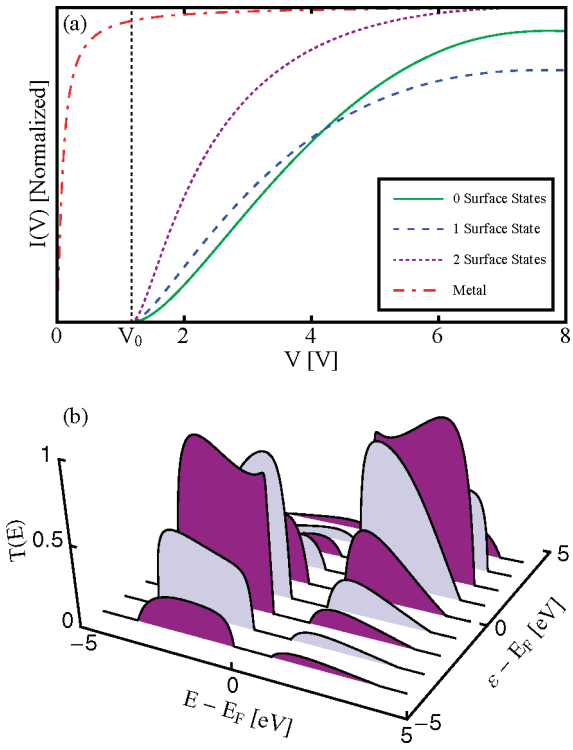

Figure 9. (a) Current−voltage profiles for molecular transport junctions with two gold (red, dot−dashed line) and two silicon electrodes. The molecular site levels are at the Fermi levels of their respective junctions, causing the metal−metal line to rise quickly for small voltages. Silicon junctions with zero (green, solid line), one (blue, dashed line), and two (purple, dotted line) contributed surface states all display a minimum voltage threshold, V_0. Electrode states are unavailable below this threshold, and no current is observed. The currents are normalized to the maximum current for a given set of electrodes. (b) Transmission functions at various ε for a silicon−molecule−silicon junction with zero contributed surface states; see Figure 8a. This illustrates how the bending, shifting, and broadening of the resonances change their interactions with different molecular site levels. The "conservation of transmission" suggested by the presentation of Figure 8 is misleading.

into the junction; likewise, there are no states for them to occupy once transmitted to the acceptor electrode. The existence of a bias voltage threshold, V_0, is correspondingly the most prominent effect of semiconductor electrodes on the current. This threshold is the minimum applied bias voltage needed to access states in either the valence or conduction band (thereby allowing current) and is independent of the molecular site energy. Figure 9a shows the current as a function of the voltage for fixed ε, further illustrating this voltage threshold.

Recalling the asymmetry in the self-energy (eqs 27 and 28) when β_1 and β_2 are exchanged, we have three possible electrode "bonding configurations" in each junction. Noting that $|\beta| < |\beta'|$ in Table 1, one assignment possibility, where neither electrode contributes a surface state ($\beta_{1,L} = \beta_{1,R} = \beta'$), is displayed in Figure 8a,b. Second is the case of one surface state ($\beta_{1,L} = \beta$ and $\beta_{1,R} = \beta'$, or vice versa) in Figure 8c,d, and last is the case of two degenerate surface states ($\beta_{1,L} = \beta_{1,R} = \beta$) in Figure 8e,f.

As expected from the possibility of surface states and as evidenced by Figure 8, the bonding configuration has a dramatic impact on the transport, particularly when ε is in the band gap. When neither electrode contributes a surface state (Figure 8a,b), we observe broad HTRs in both bands. The HTRs are shifted away from the $E = \varepsilon$ diagonal, into the bands, and cause the double-humped current−voltage profile. With one contributed surface state (Figure 8c,d), the HTRs edge closer to the band gap. The surface state in the center of the band gap appears to contribute transmission, signaling enhanced transport through molecular energy levels in the band gap. The HTRs finally spread into the band gap with the facilitation of two surface states (Figure 8e,f). Ignoring the voltage threshold, the semiconductor transport in Figure 8f is very similar to the metal transport in Figure 7b; notably, only one hump is present in the current, centered around the Fermi level. We infer two principal effects of surface states on the transport. First, they aid transport through nearby molecular site levels (presently in the band gap). Second, as suggested by the reduction in the broadening of the HTRs with more surface states, they interfere with molecule−electrode hybridization. This reduction is further explained by the scaling of $\Sigma_{AB}(E)$ with β_2^{-2}; see Figure 4.

Having insight about the shifting and broadening of the HTRs in Figure 8, we now investigate their bending. The insets of Figure 8a,c,e each display the transmission through their respective junctions when the molecular-level shifting, $\Lambda_{AB}(E)$, is neglected. Molecular-level shifting through $\Lambda_{AB}(E)$ is responsible for both the movement of the HTR away from the diagonal as well as its contorted shape. The nonlinear shape of $\Lambda_{AB}(E)$ when $\Gamma_{AB}(E) > 0$ explains the amplified shifting near the band edges; see Figure 4. Recalling that $\Lambda_{NA}(E)$ is essentially negligible for metals, we see that semiconductors interact more strongly with the molecule; the electronic transport is influenced by the molecular-level shifts and is also sensitive to the presence of surface states.

A quick glance at the transmission contour plots in Figure 8 shows that the HTRs are bent, shifted, and broadened depending on the presence of surface states. That the HTRs span the same injection energy ranges with a single HTR per band may suggest a "conservation of transmission" through the various junctions. This visual effect is fictitious. Physical systems transmit electrons through discrete, but broadened, resonances. Only their corresponding horizontal segments in Figures 7 and 8 have meaning. For instance, a molecular site level at $\varepsilon - E_F = -3.5$ eV does not display a resonance in Figure 8a when $\Lambda_{AB}(E)$ is included (the main panel); however, a resonance appears at $E - E_F = -3.5$ eV when the shifting is neglected (the inset). For this particular level, the existence of a resonance, and thus the magnitude of transmission, is *not* conserved, despite appearances in the contour plots. To further illustrate how the transmission function changes with the molecular site level, Figure 9b shows the transmission function of Figure 8a for particular ε.

If we instead use the alternating site model and consider a TiO_2−molecule−TiO_2 junction, we encounter similar choices in bonding configuration. Here, we can choose sign(α) since only |α| is parametrized, and three similar bonding configurations arise. These bonding configurations may be loosely interpreted as the molecule bonding with titanium on both electrodes, with oxygen on both, or with one titanium and one oxygen.

Figure 10 shows that many of the trends observed in the AB model are still present. First, the band gap is again manifested by strips of zero transmission and leads to similar voltage thresholds in the currents. Second, the bonding configuration in these junctions is once again important. When the molecule is connected to the same atom type on both electrodes (both $\alpha > 0$ or both $\alpha < 0$), the degenerate surface states appear to form a system resonance at α for all ε. This leads to perfect transmission at $E = \alpha$ regardless of the molecule site level, as displayed in Figure 10a,e. While always present, these resonances become infinitely narrow as $|\varepsilon - E_F| \rightarrow \infty$ and are

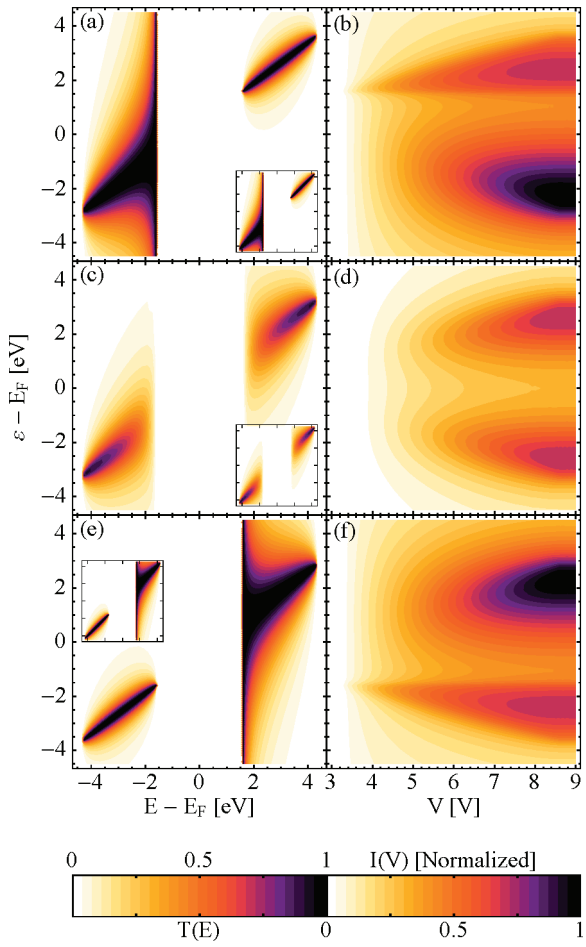

Figure 10. Transmissions (left column) and currents (right column) for junctions with two titanium dioxide electrodes. (a, b) Both electrodes connected with $\alpha < 0$; (c, d) mixed $\alpha > 0$ and $\alpha < 0$ connectivity; (e, f) both at $\alpha > 0$. As in Figure 8, we observe strips of zero transmission and a minimum bias threshold for current. The insets similarly show the transmissions with $\Lambda_{AS}(E)$ neglected, indicating the importance of molecular-level shifting due to semiconductor adsorption. The currents are normalized to the maximum current [realized in (b, f)], and the model TiO_2 parameters are listed in Table 1.

unlikely to be experimentally observed due to realistic averaging effects. Conversely, when the molecule has mixed bonding to the electrodes, Figure 10c,d, the surface states at α and $-\alpha$ appear to destroy transmission at $\pm\alpha$. We speculate that the molecule−semiconductor interfaces, recently shown to be critical in transport,[25] are responsible for these observations; however, it is not immediately obvious why or how degenerate surface states enhance transport and nondegenerate surface states dampen it.

Figure 3 shows that $\Lambda_{AS}(E)$, similar to $\Lambda_{NA}(E)$, is linear when $\Gamma_{AS}(E) > 0$. Thus, when we remove $\Lambda_{AS}(E)$ from the transmission (the insets of Figure 10a,c,e), the HTRs maintain linearity. Even without the contortions of the AB model, this shifting is still more prominent than it was in the NA model and is seen to make the HTRs more horizontal. As with the AB model, the AS model indicates that semiconductor−molecule−semiconductor junctions have strong molecular-level shiftings induced by adsorption [$\Lambda(E)$] and are sensitive to the bonding configurations at the electrode−molecule interfaces.

Conclusions

The study of electronic transport through electrode−molecule−electrode junctions has been increasing in recent years due to the interest in scanning probe microscopies, solar cells, and general molecular transport junctions. While most theoretical studies have focused exclusively on junctions with metal electrodes, experiments have also been reported for systems utilizing semiconductor electrodes. Such studies have observed negative differential resistance and asymmetric current−voltage profiles, which pose great promise for novel device construction.

In this paper, we considered extensions of the Newns−Anderson model for one-dimensional metals to one-dimensional semiconductors, where the atomic site energies and/or the interatomic site couplings were alternated. We derived the spectral densities and ultimately the total self-energies for describing molecular interactions with these one-dimensional semiconductors, including the presence of surface states. These self-energies (eqs 22 and 24) are the primary contributions of this paper and should be used instead of those from the previous paper.[41]

These models were then applied to several molecular transport junctions, and the current was calculated in the Landauer−Imry (coherent tunneling) limit. We found that a semiconductor−molecule−semiconductor junction displays a minimum bias threshold for generating current across the junction due to the electrodes' band gaps. Semiconductor−semiconductor junctions also display different molecule−electrode interactions than similar metal−metal junctions. These effects are particularly noticeable through the increased molecular-level shifting caused by adsorption to semiconductors and are very sensitive to how the molecule bonds to the semiconductor surface. Furthermore, the presence of surface states, a consequence of the bonding configuration in these models, drastically changes the electronic transport. Surface states dominate the transmission in some cases, allowing the largest currents for molecular site levels in the band gap. While discussed very generally here, the effects of these surface states on transport need to be understood in more detail. Extensions to junctions with one metal and one semiconductor electrode, subject to the "band lineup" problem, are also envisioned.

Unlike the situation for metals, molecular energy level shifting, introduced through $\Lambda(E)$, is non-negligible for semiconductors. Essentially no differences in the transmisson functions were observed between the inclusion and exclusion of $\Lambda_{NA}(E)$ for metal−metal junctions. Semiconductors, however, evidenced both bending and shifting with the inclusion of $\Lambda_{KD}(E)$ (and its AB and AS limits). This bending of the high-transmission ridges (HTRs) makes them resonant with some molecular energy levels while not with others, breaking a "conservation of transmission" seen in metal−metal junctions. While physically interesting in its own right, such an effect may also be advantageous for certain applications. Consider a molecule with a low-energy state connected between two semiconductor electrodes (without surface states, for simplicity). If this molecular state is below the HTRs, relatively low transport will be observed through the junction. When we add a gating voltage, we move the molecular level relative to the surfaces, bringing it into the range of the resonances, thereby obtaining high transport. Additional gating voltage displaces the level out of this range, reducing the current. From this, we can imagine molecular transistors. Semiconductor electrodes also invite the extension of coherent control schemes to manipulate electric current. The use of sub-band gap light and optimal control theory to command transport and device functionality holds exciting potential.

In closing, we remind the reader that many of the parameters used to model transport were qualitatively chosen, and the models' results should only be qualitatively interpreted. Due to the evidenced band gap, we believe these models capture much of the fundamental physics and chemistry of adsorption to semiconductors, although inherent errors are introduced by describing three-dimensional electrodes with one-dimensional models. A comparison of results from these one-dimensional models with those from electronic structure calculations may reveal additional information about electronic transport through molecule−semiconductor junctions.

Acknowledgment. We appreciate many enlightening discussions with Dr. Gemma C. Solomon and Prof. Vladimiro Mujica. We are grateful to the NSF [Chem and MRSEC (Grant No. DMR-0520513) programs] and the MNRF program of the DoD for support. M.G.R. acknowledges support from the DoE Computational Science Graduate Fellowship Program (Grant No. DE-FG02-97ER25308).

Appendix

Integration for $\Gamma_{KD}(E)$. The eigenvalues (eq 18) and eigenvectors (eq 21) are used in eq 2 for calculating $\Gamma_{KD}(E)$. Three change of variable substitutions are needed, $u = \alpha^2 + \beta_1^2 + \beta_2^2 + 2\beta_1\beta_2\cos(2k)$, $x = (u)^{1/2}$, and $y = -(u)^{1/2}$. Furthermore, the sign function in the eigenvalues splits the bounds of integration into two halves, $(0, \pi/2)$ and $(\pi/2, \pi)$. This split leads to an additional sign subtlety during the conversion of k to u; $\sin(2k)$ is positive for $0 < k < \pi/2$ and negative for $\pi/2 < k < \pi$. Finally

$$
\begin{aligned}
\Gamma_{KD}(E) &= \lim_{N\to\infty} 2\pi \sum_{n=1}^{N} \frac{4\gamma^2\beta_1^2 \sin^2(2k_n)\delta\left(E - \mathrm{sign}[\cos(k_n)]\sqrt{\alpha^2 + \beta_1^2 + \beta_2^2 + 2\beta_1\beta_2\cos(2k_n)}\right)}{(2N+1)[(\varepsilon_{k_n} - \alpha)^2 + \beta_1^2 + \beta_2^2 + 2\beta_1\beta_2\cos(2k_n)]} \\
&= 8\gamma^2\beta_1^2 \int_0^{\pi} \mathrm{d}k \frac{\sin^2(2k)\delta\left(E - \mathrm{sign}[\cos(k)]\sqrt{\alpha^2 + \beta_1^2 + \beta_2^2 + 2\beta_1\beta_2\cos(2k)}\right)}{(\varepsilon_k - \alpha)^2 + \beta_1^2 + \beta_2^2 + 2\beta_1\beta_2\cos(2k)} \\
&= 8\gamma^2\beta_1^2 \int_0^{\pi/2} \mathrm{d}k \frac{\sin^2(2k)\delta\left(E - \sqrt{\alpha^2 + \beta_1^2 + \beta_2^2 + 2\beta_1\beta_2\cos(2k)}\right)}{(\sqrt{\alpha^2 + \beta_1^2 + \beta_2^2 + 2\beta_1\beta_2\cos(2k)} - \alpha)^2 + \beta_1^2 + \beta_2^2 + 2\beta_1\beta_2\cos(2k)} + \\
&\quad 8\gamma^2\beta_1^2 \int_{\pi/2}^{\pi} \mathrm{d}k \frac{\sin^2(2k)\delta\left(E + \sqrt{\alpha^2 + \beta_1^2 + \beta_2^2 + 2\beta_1\beta_2\cos(2k)}\right)}{(-\sqrt{\alpha^2 + \beta_1^2 + \beta_2^2 + 2\beta_1\beta_2\cos(2k)} - \alpha)^2 + \beta_1^2 + \beta_2^2 + 2\beta_1\beta_2\cos(2k)} \\
&= \frac{-\gamma^2}{\beta_2^2} \int_{\alpha^2+(\beta_1-\beta_2)^2}^{\alpha^2+(\beta_1+\beta_2)^2} \mathrm{d}u \frac{\delta(E - \sqrt{u})\sqrt{[\alpha^2 + (\beta_1+\beta_2)^2 - u][u - \alpha^2 - (\beta_1+\beta_2)^2]}}{(\sqrt{u} - \alpha)^2 + u - \alpha^2} - \\
&\quad \frac{\gamma^2}{\beta_2^2} \int_{\alpha^2+(\beta_1-\beta_2)^2}^{\alpha^2+(\beta_1+\beta_2)^2} \mathrm{d}u \frac{\delta(E + \sqrt{u})(-1)\sqrt{[\alpha^2 + (\beta_1+\beta_2)^2 - u][u - \alpha^2 - (\beta_1+\beta_2)^2]}}{(-\sqrt{u} - \alpha)^2 + u - \alpha^2} \\
&= \frac{\gamma^2}{\beta_2^2} \int_{\sqrt{\alpha^2+(\beta_1-\beta_2)^2}}^{\sqrt{\alpha^2+(\beta_1+\beta_2)^2}} \mathrm{d}x \frac{\delta(E - x)\sqrt{[\alpha^2 + (\beta_1+\beta_2)^2 - x^2][x^2 - \alpha^2 - (\beta_1+\beta_2)^2]}}{x - \alpha} - \\
&\quad \frac{\gamma^2}{\beta_2^2} \int_{-\sqrt{\alpha^2+(\beta_1-\beta_2)^2}}^{-\sqrt{\alpha^2+(\beta_1+\beta_2)^2}} \mathrm{d}y \frac{\delta(E - y)\sqrt{[\alpha^2 + (\beta_1+\beta_2)^2 - y^2][y^2 - \alpha^2 - (\beta_1+\beta_2)^2]}}{y - \alpha} \\
&= \frac{\gamma^2}{\beta_2^2}\sqrt{\frac{[\alpha^2 + (\beta_1+\beta_2)^2 - E^2][E^2 - \alpha^2 - (\beta_1-\beta_2)^2]}{(E - \alpha)^2}}
\end{aligned}
$$

for $[\alpha^2 + (\beta_1 - \beta_2)^2]^{1/2} \le |E| \le [\alpha^2 + (\beta_1 + \beta_2)^2]^{1/2}$. $\Gamma_{KD}(E) = 0$ for all other E.

References and Notes

(1) O'Regan, B.; Grätzel, M. *Nature* **1991**, *353*, 737–740.

(2) Nitzan, A. *Chemical Dynamics in Condensed Phases: Relaxation, Transfer, and Reactions in Condensed Molecular Systems*; Oxford University Press: New York, 2006.

(3) Nitzan, A. *Annu. Rev. Phys. Chem.* **2001**, *52*, 681–750.

(4) Datta, S. *Quantum Tranport: Atom to Transistor*; Cambridge University Press: New York, 2005.

(5) *Introducing Molecular Electronics*; Cuniberti, G., Richter, K., Fagas, G., Eds.; Springer-Verlag: New York, 2005.

(6) Di Ventra, M. *Electrical Transport in Nanoscale Systems*; Cambridge University Press: New York, 2008.

(7) *J. Phys.: Condens. Matter* **2008**, *20*. A special issue that provides an excellent collection of articles on "The conductivity of single molecules and supramolecular architectures".

(8) Magoga, M.; Joachim, C. *Phys. Rev. B* **1997**, *56*, 4722–4729.

(9) Yaliraki, S. N.; Ratner, M. A. *J. Chem. Phys.* **1998**, *109*, 5036–5043.

(10) Emberly, E. G.; Kirczenow, G. *Phys. Rev. B* **1998**, *58*, 10911–10920.

(11) Hall, L. E.; Reimers, J. R.; Hush, N. S.; Silverbrook, K. *J. Chem. Phys.* **2000**, *112*, 1510–1521.

(12) Hipps, K. W. *Science* **2001**, *294*, 536–537.

(13) Hihath, J.; Arroyo, C. R.; Rubio-Bollinger, G.; Tao, N.; Agraït, N. *Nano Lett.* **2008**, *8*, 1673–1678.

(14) Kristensen, I. S.; Mowbray, D. J.; Thygesen, K. S.; Jacobsen, K. W. *J. Phys.: Condens. Matter* **2008**, *20*, 374101.

(15) Tian, W.; Datta, S.; Hong, S.; Reifenberger, R.; Henderson, J. I.; Kubiak, C. P. *J. Chem. Phys.* **1998**, *109*, 2874–2882.

(16) Metzger, R. M.; Xu, T.; Peterson, I. R. *J. Phys. Chem. B* **2001**, *105*, 7280–7290.

(17) Ward, D. R.; Halas, N. J.; Ciszek, J. W.; Tour, J. M.; Wu, Y.; Nordlander, P.; Natelson, D. *Nano Lett.* **2008**, *8*, 919–924.
(18) McCreery, R.; Dieringer, J.; Solak, A. O.; Snyder, B.; Nowak, A. M.; McGovern, W. R.; Duvall, S. *J. Am. Chem. Soc.* **2003**, *125*, 10748–10758.
(19) Guisinger, N. P.; Greene, M. E.; Basu, R.; Baluch, A. S.; Hersam, M. C. *Nano Lett.* **2004**, *4*, 55–59.
(20) Guisinger, N. P.; Yoder, N. L.; Hersam, M. C. *Proc. Natl. Acad. Sci. U.S.A.* **2005**, *102*, 8838–8843.
(21) Piva, P. G.; DiLabio, G. A.; Pitters, J. L.; Zikovsky, J.; Rezeq, M.; Dogel, S.; Hofer, W. A.; Wolkow, R. A. *Nature* **2005**, *435*, 658–661.
(22) Yoder, N. L.; Guisinger, N. P.; Hersam, M. C.; Jorn, R.; Kaun, C.-C.; Seideman, T. *Phys. Rev. Lett.* **2006**, *97*, 187601.
(23) Rakshit, T.; Liang, G.-C.; Ghosh, A. W.; Datta, S. *Nano Lett.* **2004**, *4*, 1803–1807.
(24) Rakshit, T.; Liang, G.-C.; Ghosh, A. W.; Hersam, M. C.; Datta, S. *Phys. Rev. B* **2005**, *72*, 125305.
(25) Yu, L. H.; Gergel-Hackett, N.; Zangmeister, C. D.; Hacker, C. A.; Richter, C. A.; Kushmerick, J. G. *J. Phys.: Condens. Matter* **2008**, *20*, 374114.
(26) Hovis, J. S.; Liu, H.; Hamers, R. J. *Surf. Sci.* **1998**, *402*−*404*, 1–7.
(27) Wolkow, R. A. *Annu. Rev. Phys. Chem.* **1999**, *50*, 413–441.
(28) Kirczenow, G.; Piva, P. G.; Wolkow, R. A. *Phys. Rev. B* **2005**, *72*, 245306.
(29) Leftwich, T. R.; Madachik, M. R.; Teplyakov, A. V. *J. Am. Chem. Soc.* **2008**, *130*, 16216–16223.
(30) Reuter, M. G.; Sukharev, M.; Seideman, T. *Phys. Rev. Lett.* **2008**, *101*, 208303.
(31) Landauer, R. *IBM J. Res. Dev.* **1957**, *1*, 223–231.
(32) Landauer, R. *Philos. Mag.* **1970**, *21*, 863–867.
(33) Imry, Y. In *Directions in Condensed Matter Physics*; Grinstein, G., Mazenko, G., Eds.; World Scientific: River Edge, NJ, 1986; pp 101−163.
(34) Cahay, M.; McLennan, M.; Datta, S. *Phys. Rev. B* **1988**, *37*, 10125–10136.
(35) Jauho, A.-P.; Wingreen, N. S.; Meir, Y. *Phys. Rev. B* **1994**, *50*, 5528–5544.
(36) Newns, D. M. *Phys. Rev.* **1969**, *178*, 1123–1135.
(37) Anderson, P. W. *Phys. Rev.* **1961**, *124*, 41–53.
(38) Koutecký, J. *Adv. Chem. Phys.* **1965**, *9*, 85–168.
(39) Foo, E. N.; Davison, S. G. *Surf. Sci.* **1976**, *55*, 274–284.
(40) Petersson, Å.; Ratner, M.; Karlsson, H. O. *J. Phys. Chem. B* **2000**, *104*, 8498–8502.
(41) Mujica, V.; Ratner, M. A. *Chem. Phys.* **2006**, *326*, 197–203.
(42) Haydock, R.; Heine, V.; Kelly, M. J. *J. Phys. C* **1972**, *5*, 2845–2858.
(43) Cini, M. *Topics and Methods in Condensed Matter Theory*; Springer-Verlag: New York, 2007.
(44) In full generality, $G_{elec}(E)$ is a matrix, requiring two indices for a specific element. Presently, we only need the diagonal elements; therefore, the second index is omitted.
(45) Xue, Y.; Datta, S.; Ratner, M. A. *J. Chem. Phys.* **2001**, *115*, 4292–4299.
(46) Meir, Y.; Wingreen, N. S. *Phys. Rev. Lett.* **1992**, *68*, 2512–2515.
(47) Foo, E.-N.; Wong, H.-S. *Phys. Rev. B* **1974**, *9*, 1857–1860.
(48) Muscat, J. P.; Davison, S. G.; Liu, W. K. *J. Phys. Chem.* **1983**, *87*, 2977–2981.
(49) Tamm, I. *Phys. Z. Sowjetunion* **1933**, *1*, 733–746.
(50) Shockley, W. *Phys. Rev.* **1939**, *56*, 317–323.
(51) Dy, K. S.; Wu, S.-Y.; Spratlin, T. *Phys. Rev. B* **1979**, *20*, 4237–4243.
(52) Crain, J. N.; Pierce, D. T. *Science* **2005**, *307*, 703–706.
(53) We note that $\sin[k_n(2N + 1)]$ in the Newns−Anderson case is not equivalent to $\sin[2k_nN] + \sin[2k_n(N + 1)]$ here; however, they share the same roots.
(54) The quantization condition for the KD model, eq 20, can be rewritten as $\mu \sin[2k_n(N + 1)] + \sin(2k_nN) = 0$, where $\mu \equiv \beta_1/\beta_2$. It can be verified that $k_n = n\pi/(2N + 1)$ when $\mu = 1$. When $\mu \rightarrow 0$, we get $k_n \rightarrow n\pi/2N$, and when $\mu \rightarrow \infty$, $k_n \rightarrow n\pi/(2N + 2)$. We then infer that the k_n are roughly evenly spaced (independent of μ) and that the spacing is approximately $\pi/(2N + 1)$.
(55) The reduction of $[E^2-\alpha^2-(\beta_1-\beta_2)^2]^{1/2}$ to $|E|$ in this combined limit creates the sign disparity observed in $\Theta_{NA}(E)$.
(56) Mujica, V.; Kemp, M.; Ratner, M. A. *J. Chem. Phys.* **1994**, *101*, 6956–6864.

JP811492U